

# Eyeglasses-free Display: Towards Correcting Visual Aberrations with Computational Light Field Displays

Fu-Chung Huang<sup>1,4</sup>

Gordon Wetzstein<sup>2</sup>

Brian A. Barsky<sup>1,3</sup>

Ramesh Raskar<sup>2</sup>

<sup>1</sup>Computer Science Division, UC Berkeley <sup>2</sup>MIT Media Lab <sup>3</sup>School of Optometry, UC Berkeley <sup>4</sup>Microsoft Corporation

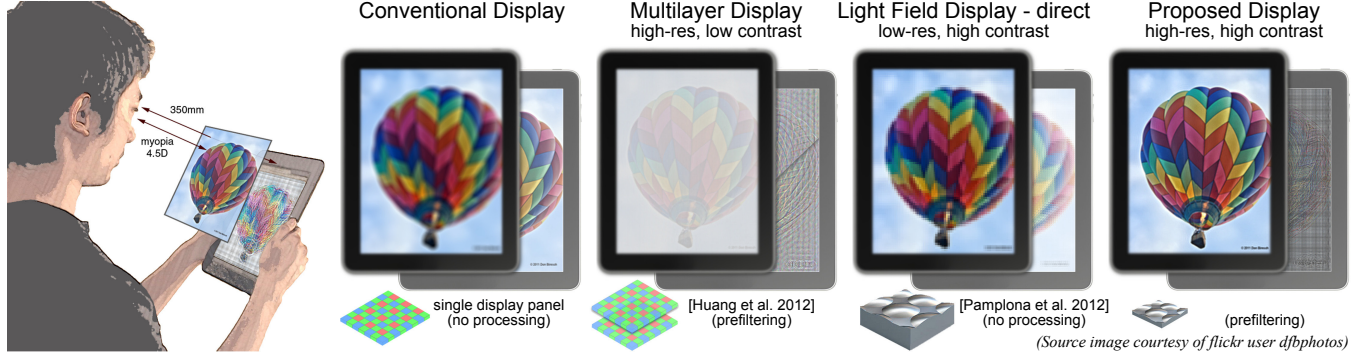


**Figure 1:** Vision correction with computational displays. On a conventional screen, people with optical aberrations see a blurred image (center left). Current approaches to aberration-correcting display use multilayer prefilters (center) or light field displays (center right). While the former technology enhances perceived image sharpness, contrast is severely reduced. Existing light field-based solutions offer high contrast but require a very high angular sampling density, which significantly reduces image resolution. In this paper, we explore the convergence of light field display optics and computational prefilters (right), which achieves high image resolution and contrast simultaneously.

## Abstract

Millions of people worldwide need glasses or contact lenses to see or read properly. We introduce a computational display technology that predistorts the presented content for an observer, so that the target image is perceived without the need for eyewear. By designing optics in concert with prefilters, the proposed display architecture achieves significantly higher resolution and contrast than prior approaches to vision-correcting image display. We demonstrate that inexpensive light field displays driven by efficient implementations of 4D prefilters can produce the desired vision-corrected imagery, even for higher-order aberrations that are difficult to be corrected with glasses. The proposed computational display architecture is evaluated in simulation and with a low-cost prototype device.

**CR Categories:** B.4.2 [Hardware]: Input/Output and Data Communications—Image display; H.1.2 [Information Systems]: User/Machine Systems—Human factors; I.3.3 [Computer Graphics]: Picture/Image Generation—Display algorithms;

**Keywords:** computational ophthalmology, displays, light fields

**Links:** [DL](#) [PDF](#) [WEB](#) [VIDEO](#) [DATA](#) [CODE](#)

## 1 Introduction

Today, an estimated 41.6% of the US population [Vitale et al. 2009] and more than half of the population in some Asia countries [Wong et al. 2000] suffer from myopia. Eyeglasses have been the primary tool to correct such aberrations since the 13th century. Recent decades have seen contact lenses and refractive surgery supplement available options to correct for refractive errors. Unfortunately, all of these approaches are intrusive in that the observer either has to use eyewear or undergo surgery, which can be uncomfortable or even dangerous.

Within the last year, two vision-correcting computational display architectures have been introduced as non-intrusive alternatives. Pamplona et al. [2012] proposed to use light field displays to enable the display to correct the observer’s visual aberrations. This correction relies on a 2D image to be shown within the observer’s focal range, outside the physical display enclosure. Light field displays offering such capabilities require extremely high angular sampling rates, which significantly reduce spatial image resolution. As a high-resolution alternative, Huang et al. [2012] proposed a multilayer device that relies on prefiltered image content. Unfortunately, the required prefilters for these particular optical configurations drastically reduce image contrast. In this paper, we explore combinations of viewer-adaptive prefilters with off-the-shelf lenslets or parallax barriers and demonstrate that the resulting vision-correcting computational display system facilitates significantly higher contrast and resolution as compared to previous solutions (see Fig. 1).

While light field displays have conventionally been used for glasses-free 3D image presentation, correcting for visual aberrations of observers is a promising new direction with direct benefits for millions of people. We believe that our approach is the first to make such displays practical by providing both high resolution and contrast—the two design criteria that have been driving the display industry for the last decade. We envision future display systems to be integrated systems comprising flexible optical con-

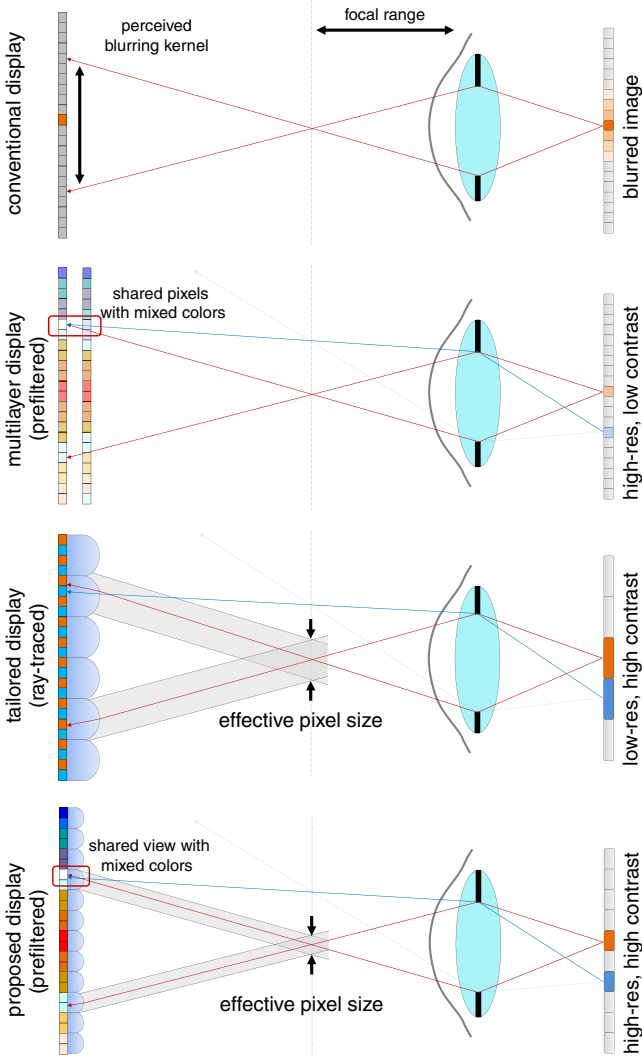


**Figure 2:** Illustration of vision-correcting displays. Observing a conventional 2D display outside the focal range of the eye results in a blurred image (top). A multilayer display with prefiltered image generation (second row) allows for improved image sharpness at the cost of reduced contrast. Image contrast can be preserved using a light field approach via lenslet arrays on the screen (third row); this approach severely reduces image resolution. Combining light field display and computational prefiltering, as proposed in this paper (bottom), allows for vision-correcting image display with significantly improved image resolution and contrast.

figurations combined with sophisticated computing that allow for different modes, such as 2D, glasses-free 3D, or vision-correcting image display.

We explore computational displays with applications in correcting visual aberrations of human observers. In particular, we make the following contributions:

- We introduce a novel vision-correcting computational display system that leverages readily available hardware components in concert with light field prefiltering algorithms.
- We analyze vision-correcting displays in the frequency domain and show that light field displays provide fundamentally more degrees of freedom than other approaches.

- We demonstrate that light field prefiltering offers benefits over alternative vision-correcting displays: image resolution and contrast are significantly enhanced; implementations with parallax barriers are brighter and lenslet-based devices have thinner form factors.
- We evaluate the proposed display system using a wide range of simulations and build a low-cost prototype device that demonstrates correction of myopia and hyperopia in practice.

### 1.1 Overview of Limitations

The proposed system requires modifications to conventional display hardware and increased computational resources. Although our displays provide significant benefits over previous work, small tradeoffs in both resolution and contrast have to be made compared to conventional 2D displays. We evaluate the prototype using photographs taken with aperture settings corresponding to those of the human eye and with simulations using computational models of human perception. However, we do not run a full-fledged user study. A commercial implementation of the proposed technology may require eye tracking, which is outside the scope of this paper. Our academic display prototype exhibits color artifacts that are due to moiré between the parallax barrier and the display subpixels. These artifacts could be removed with diffusing films tailored for the subpixel structure of the screen. Finally, the employed parallax barriers reduce image brightness.

## 2 Related Work

**Light Fields and Computational Ophthalmology** Since their introduction to computer graphics, light fields [Levoy and Hanrahan 1996; Gortler et al. 1996] have become one of the most fundamental tools in computational photography. Frequency analyses [Durand et al. 2005], for instance, help better understand the theoretical foundations of ray-based light transport whereas applications range from novel camera designs, e.g. [Levin et al. 2009], and aberration correction in light field cameras [Ng and Hanrahan 2006], to low-cost devices that allow for diagnosis of refractive errors [Pamplona et al. 2010] or cataracts [Pamplona et al. 2011] in the human eye. These applications are examples of computational ophthalmology, where interactive techniques are combined with computational photography and display for medical applications.

**Light Field Displays** Glasses-free 3D or light field displays were invented in the beginning of the 20th century. The two dominating technologies are lenslet arrays [Lippmann 1908] and parallax barriers [Ives 1903]. Today, a much wider range of different 3D display technologies are available, including volumetric displays [Cossart et al. 2007; Jones et al. 2007], multifocal displays [Akeley et al. 2004; Love et al. 2009], and super-multi-view displays [Takaki 2006]. Volumetric displays create the illusion of a virtual 3D object floating inside the physical device enclosure; an observer can accommodate within this volume. Multifocal displays allow for the display of imagery on different focal planes but require either multiple devices in a large form factor [Akeley et al. 2004] or vary-focal glasses to be worn [Love et al. 2009]. Super-multi-view displays emit light fields with an extremely high angular resolution, which is achieved by employing many spatial light modulators. Most recently, near-eye light field displays [Lanman and Luebke 2013] and compressive light field displays [Lanman et al. 2010; Wetzstein et al. 2012; Maimone et al. 2013; Hirsch et al. 2014] have been introduced. With the exception of [Maimone et al. 2013], none of these technologies is demonstrated to support accommodation. A recent survey of computational displays can be found in Masia et al. [2013].

Building light field displays that support all depth cues, including binocular disparity, motion parallax, and accommodation, in a thin form factor is one of the most challenging problem in display design today. The support for accommodation allows an observer to focus on virtual images that float at a distance to the physical device. This capability would allow for the correction of low-order visual aberrations, such as myopia and hyperopia. Maimone et al. [2013] demonstrate the first single-device solution for this problem that does not require glasses; their device form-factor is—unlike ours—not suitable for mobile displays. We propose a different strategy: rather than aiming for the support of all depth cues with a single device, we employ simple parallax barriers or lenslet arrays with a very narrow field of view to *only* support accommodation, but not binocular disparity or motion parallax. That means glasses-free 3D display may not be possible with the proposed devices. However, our approach allows us to use inexpensive add-ons to existing phones or tablets, facilitating eyeglasses-free 2D image display for observers with visual aberrations, including myopia, hyperopia, astigmatism, and higher-order aberrations.

**Vision-correcting Displays** Devices tailored to correct visual aberrations of human observers have recently been introduced. Early approaches attempt to pre-sharpen a 2D image presented on a conventional screen with the inverse point spread function (PSF) of the observer’s eye [Alonso Jr. and Barreto 2003; Yellott and Yellott 2007; Archand et al. 2011]. Although these methods slightly improve image sharpness, the problem itself is ill-posed. Fundamentally, the PSF of an eye with refractive errors is usually a low-pass filter—high image frequencies are irreversibly canceled out in the optical path from display to the retina. To overcome this limitation, Pamplona et al. [2012] proposed the use of 4D light field displays with lenslet arrays or parallax barriers to correct visual aberrations. For this application, the emitted light fields must provide a sufficiently high angular resolution so that multiple light rays emitted by a single lenslet enter the same pupil (see Fig. 2). This approach can be interpreted as lifting the problem into a higher-dimensional (light field) space, where the inverse problem becomes well-posed.

Unfortunately, conventional light field displays as used by Pamplona et al. [2012] are subject to a spatio-angular resolution trade-off: an increased angular resolution decreases the spatial resolution. Hence, the viewer sees a sharp image but at a significantly lower resolution than that of the screen. To mitigate this effect, Huang et al. [2011; 2012] recently proposed to use multilayer display designs together with prefiltering. While this is a promising, high-resolution approach, combining prefiltering and these particular optical setups significantly reduces the resulting image contrast.

Pamplona et al. [2012] explore the resolution-limits of available hardware to build vision-correcting displays; Huang et al. [2011; 2012] show that computation can be used to overcome the resolution limits, but at the cost of decreased contrast. The approach proposed in this paper combines both methods by employing 4D light field prefiltering with hardware designs that have previously only been used in a “direct” way, i.e. each screen pixel corresponds to one emitted light ray. We demonstrate that this design allows for significantly higher resolutions as compared to the “direct” method because angular resolution demands are decreased. At the same time, image contrast is significantly increased, compared to previous prefiltering approaches, because of the hardware we use.

### 3 Light Field Transport and Inversion

In this section, we derive the optical image formation of a light field on the observer’s retina as well as image inversion methods. For this purpose, we employ a two-plane parameterization [Levoy and Hanrahan 1996; Chai et al. 2000] of the light fields emitted by

the device and inside the eye. The forward and inverse models in this section are derived for two-dimensional “flatland” light fields with straightforward extensions to the full four-dimensional formulations.

#### 3.1 Retinal Light Field Projection

We define the lateral position on the retina to be  $x$  and that on the pupil to be  $u$  (see Fig. 3). The light field  $l(x, u)$  describes the radiance distribution inside the eye. Photoreceptors in the retina average over radiance incident from all angles; therefore, the perceived intensity  $i(x)$  is modeled as the projection of  $l$  along its angular dimension:

$$i(x) = \int_{\Omega_u} l(x, u) du, \quad (1)$$

where  $\Omega_u$  is the integration domain, which is limited by the finite pupil size. Vignetting and other angle-dependent effects are absorbed in the light field. Assuming that the display is capable of emitting a light field that contains spatial variation over the screen plane  $x^d$  and angular variation over the pupil plane  $u^d$ , allows us to model the radiance distribution entering the eye as a light field  $l^d(x^d, u^d)$ . Note that the coordinates on the pupil plane for the light fields inside the eye and on the display are equivalent ( $u \triangleq u^d$ ).

Refractions and aberrations in the eye are modeled as a mapping function  $\phi : \mathbb{R} \times \mathbb{R} \rightarrow \mathbb{R}$  from the spatio-angular coordinates of  $l$  to a location on the screen, such that  $x^d = \phi(x, u)$ . Equation 1 therefore becomes

$$i(x) = \int_{-\infty}^{\infty} l^d(\phi(x, u), u) A(u) du. \quad (2)$$

Here, the effect of the finite pupil diameter  $r$  is a multiplication of the light field with the pupil function  $A(u) = \text{rect}(\frac{u}{r})$ . In the full 4D case, the *rect* function is replaced by a circular function modeling the shape of the pupil.

Following standard ray transfer matrix notation [Hecht 2001], the mapping between rays incident on the retina and those emitted by the screen can be modeled as the combined effect of transport between retina and pupil by distance  $D^e$ , refraction of the lens with focal length  $f$ , and transport between pupil and screen by distance  $D^o$ . In matrix notation, this transformation is expressed as

$$\begin{pmatrix} \phi(x, u) \\ u^d \end{pmatrix} = \begin{pmatrix} -\frac{D^o}{D^e} & D^o \Delta \\ 0 & 1 \end{pmatrix} \begin{pmatrix} x \\ u \end{pmatrix} = \mathbf{T} \begin{pmatrix} x \\ u \end{pmatrix} \quad (3)$$

where  $\mathbf{T}$  is the concatenation of the individual propagation operators and  $\Delta = \frac{1}{D^e} - \frac{1}{f} + \frac{1}{D^o}$ . We derive Equation 3 in Supplemental Section A. As a first-order approximation, Equation 3 only models the defocus of the eye by considering its focal length  $f$ , which may be constrained due to the observer’s limited accommodation range. However, astigmatism and higher-order aberrations can be included in this formulation (see Sec. 6.2).

Discretizing Equations 2 and 3 results in a linear forward model:

$$\mathbf{i} = \mathbf{P} \mathbf{l}^d, \quad (4)$$

where the matrix  $\mathbf{P} \in \mathbb{R}^{N \times N}$  encodes the projection of the discrete, vectorized 4D light field  $\mathbf{l}^d \in \mathbb{R}^N$  emitted by the display onto the retina  $\mathbf{i} \in \mathbb{R}^N$ . For the remainder of the paper, we assume that the number of emitted light rays  $N$  is the same as the discretized locations on the retina, which makes  $\mathbf{P}$  square.

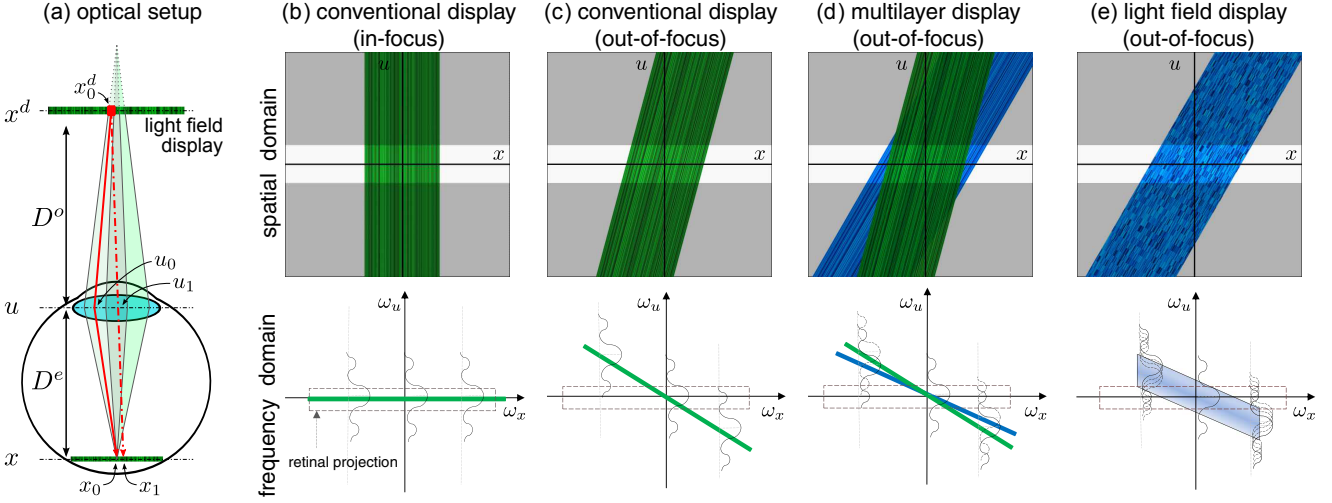


**Figure 3:** Light field analysis for different displays. The light field emitted by a display is parameterized by its coordinates on the screen  $x^d$ , on the pupil  $u$ , and on the retina  $x$  (a). This light field propagates through the pupil and is projected into a 2D image on the retina. For an in-focus display, the light field incident on the retina is a horizontal line in the frequency domain (b). For a displayed image outside of the accommodation range of the observer, the corresponding light field is slanted and energy is lost at some spatial frequencies (c). Multilayer displays utilize an additional display layer to preserve all spatial frequencies (d). With light field displays, frequency loss is also avoided; the perceived image frequencies are a combination of all spatio-angular frequencies of the incident light field (e). The ray paths in (a) show two effects for a hyperopic eye observing a light field display. First, each photoreceptor on the retina averages over multiple neighboring pixels on the screen (green shaded regions). Second, each pixel on the screen (e.g.,  $x_0^d$ ) emits different intensities toward different regions on the pupil ( $u_0, u_1$ ), allowing the same pixel to appear differently when observed from different locations ( $x_0, x_1$ ) on the retina (red arrows).

### 3.2 Inverse Light Field Projection

The objective of an aberration-correcting display is to present a 4D light field to the observer, such that a desired 2D retinal projection is perceived. Assuming that viewing distance, pupil size, and other parameters are known, the emitted light field can be found by optimizing the following objective function:

$$\begin{aligned} & \underset{\{\mathbf{l}^d\}}{\text{minimize}} \quad \|\mathbf{i} - \mathbf{P}\mathbf{l}^d\|_2 \\ & \text{subject to} \quad 0 \leq l_i^d \leq 1, \quad \text{for } i = 1 \dots N \end{aligned} \quad (5)$$

Here,  $\mathbf{i}$  is the target image (given in normalized power per unit area) and the constraints of the objective account for physically feasible pixel states of the screen. Equation 5 can be solved using standard non-negative linear solvers, we employ LBFGS-B [Byrd et al. 1995]. As shown in the following frequency interpretation and in Section 4, Equation 5 is an ill-posed problem for conventional 2D displays. The problem becomes invertible through the use of 4D light field displays.

### 3.3 Frequency Domain Analysis

While Equation 5 allows for optimal display pixels states to be determined, a natural question that remains is ‘Which display type is best suited for aberration-correction?’. We attempt to answer this question in two different ways: with a frequency analysis derived in this section and with an analysis of the conditioning of projection matrix  $\mathbf{P}$  in Section 4.

Frequency analyses have become standard tools to generate an intuitive understanding of performance bounds of computational cameras and displays (e.g., [Durand et al. 2005; Levin et al. 2009; Wetzelstein et al. 2011]), we follow this approach. First, we note that the coordinate transformation  $\mathbf{T}$  between display and retina can be used to model corresponding transformation in the frequency domain via the Fourier linear transformation theorem:

$$\begin{pmatrix} \omega_x^d \\ \omega_u^d \end{pmatrix} = \begin{pmatrix} -\frac{D^e}{D^o \Delta} & 0 \\ 1 & 1 \end{pmatrix} \begin{pmatrix} \omega_x \\ \omega_u \end{pmatrix} = \hat{\mathbf{T}} \begin{pmatrix} \omega_x \\ \omega_u \end{pmatrix}, \quad (6)$$

where  $\omega_x, \omega_u$  are the spatial and angular frequencies of the light field inside the eye,  $\omega_x^d, \omega_u^d$  the corresponding frequencies on the display, and  $\hat{\mathbf{T}} = \mathbf{T}^{-T}$  [Ramamoorthi et al. 2007].

One of the most interesting results of the frequency analysis is the effect of the pupil outlined in Equation 2. The multiplication with the pupil function in the spatial domain becomes a convolution in the frequency domain whereas the projection along the angular dimension becomes a slicing [Ng 2005] along  $\omega_u = 0$ :

$$\begin{aligned} \hat{i}(\omega_x) &= (\hat{l} * \hat{A})(\omega_x, 0) = \int_{\Omega_{\omega_u}} \hat{l}(\omega_x, \omega_u) \hat{A}(\omega_u) d\omega_u \\ &= \int_{\Omega_{\omega_u}} \hat{l}^d \left( -\frac{D^e}{D^o} \omega_x, D^e \Delta \omega_x + \omega_u \right) \hat{A}(\omega_u) d\omega_u. \end{aligned} \quad (7)$$

Here,  $\hat{\cdot}$  denotes the Fourier transform of a variable and  $\hat{A}(\omega_u) = \text{sinc}(r\omega_u)$ . Note that the convolution with the sinc function accumulates higher angular frequencies along  $\omega_u = 0$  before the slicing occurs, so those frequencies are generally preserved but are all mixed together (see Figs. 3 b-e).

**Conventional 2D Displays** Equation 7 is the most general formulation for the perceived spectrum of an emitted light field. The light field that can actually be emitted by certain types of displays, however, may be very restricted. In a conventional 2D display, for instance, each pixel emits light isotropically in all directions, which makes the emitted light field constant in angle. Its Fourier transform is therefore a Dirac in the angular frequencies (i.e.  $\hat{l}^d(\omega_x^d, \omega_u^d) = 0 \forall \omega_u^d \neq 0$ ).

Taking a closer look at Equation 7 with this restriction in mind, allows us to disregard all non-zero angular frequencies of the displayed light field and focus on  $\omega_u^d = D^e \Delta \omega_x + \omega_u = 0$ . As illustrated in Figures 3 (b-c, bottom), the light field incident on the retina is therefore a line  $\omega_u = -D^e \Delta \omega_x$ , which we can parameterize by its slope  $s = -D^e \Delta$ . Equation 7 simplifies to

$$\hat{i}_{2D}(\omega_x) = \hat{l}^d \left( -\frac{D^e}{D^o} \omega_x, 0 \right) \text{sinc}(r s \omega_x). \quad (8)$$

Unfortunately, *sinc* functions contain a lot of zero-valued positions, making the correction of visual aberrations with 2D displays an ill-posed problem.

**Correction with Multilayer Prefiltering** Huang et al. [2012] proposed to remedy this ill-posedness by adding an additional layer, such as a liquid crystal display, to the device. Although stacks of liquid crystal panels usually result in a multiplicative image formation (Wetzstein et al. [2011; 2012]), Huang et al. propose to multiplex the displayed patterns in time, which results in an additive image formation because of perceptual averaging via persistence of vision. As illustrated in Figure 3 (d), this changes the frequency domain representation to the sum of two lines with different slopes. Generalizing Equation 8 to multiple display layers results in the following frequency representation of the retinal projection:

$$\hat{i}_{ml}(\omega_x) = \sum_k \hat{l}^{(d,k)} \left( -\frac{D^e}{D^{(o,k)}} \omega_x, 0 \right) \text{sinc}(rs^{(k)} \omega_x), \quad (9)$$

where  $s^{(k)}$  is the slope of display layer  $k$  and  $\hat{l}^{(d,k)}$  is the light field emitted by that layer. The offsets between display layers are chosen so that the envelope of the differently sheared *sinc* functions contains no zeros. While this is conceptually effective, physical constraints of the display, such as nonnegative pixel states and limited dynamic range, result in a severe loss of contrast in practice.

**Correction with Light Field Displays** As opposed to 2D displays or multilayer displays, light field displays have the capability to generate a continuous range of spatio-angular frequencies. Basically, this allows for multiple virtual 2D layers to be emitted simultaneously, each having a different slope  $\tilde{s}$  (see Fig. 3 e). Following the intuition used in Equations 8 and 9, we can write Equation 7 as

$$\begin{aligned} \hat{i}_{lf}(\omega_x) &= \int_{\Omega_{\tilde{s}}} \hat{l}(\omega_x, \tilde{s}\omega_x) \hat{A}(\tilde{s}\omega_x) d\tilde{s} \\ &= \int_{\Omega_{\tilde{s}}} \hat{l}^d \left( -\frac{D^e}{D^o} \omega_x, D^e \Delta \omega_x + \tilde{s}\omega_x \right) \text{sinc}(r\tilde{s}\omega_x) d\tilde{s}. \end{aligned} \quad (10)$$

Although Equation 10 demonstrates that light field displays support a wide range of frequencies, many different solutions for actually computing them for a target image exist. Pamplona et al. [2012] chose a naive ray-traced solution. Light field displays, however, offer significantly more degrees of freedom, but these are only unlocked by solving the full inverse light field projection problem (Eq. 5), which we call ‘‘light field prefiltering’’. We demonstrate that this approach provides significant improvements in image resolution and contrast in the following sections.

## 4 Analysis

Whereas the previous section introduces forward and inverse image formation and also provides an interpretation in the frequency domain, we analyze results and capabilities of the proposed method in this section. First, we give an intuitive explanation for when the problem of correcting visual aberrations is actually invertible, and

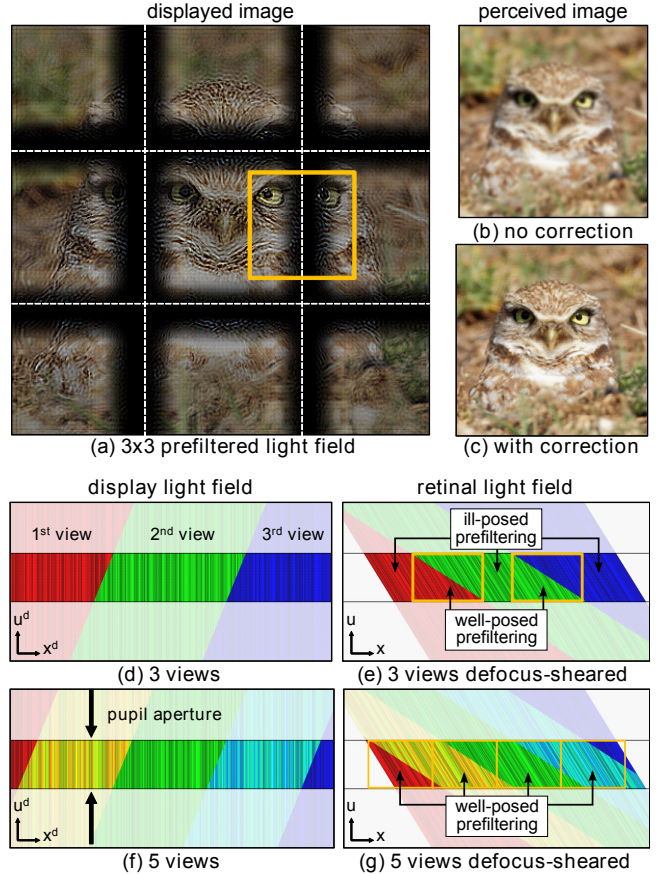


**Figure 4:** Light field prefiltering. The proposed prefiltering approach computes a light field (here with  $3 \times 3$  views) that results in a desired 2D projection on the retina of an observer. The prefiltered light field for an example scene is shown in (a), its simulated projection on the retina in (c), and an image observed on a conventional screen in (b). Spatio-angular frequencies of the light field are amplified, resulting in the desired sharpening when integrated on the retina. Two sample ‘‘flatland’’ light fields with different angular sampling rates are shown in display (d,f) and in eye (e,g) coordinates. Here, the yellow boxes illustrate why 4D light field prefiltering is more powerful than 2D image prefiltering: a single region on the retina receives contributions from multiple different light field views (e,g). Wherever that is the case, the inverse problem of light field prefiltering is well-posed but in other regions the problem is the same as the ill-posed problem faced with conventional 2D displays (e). (Source image courtesy of Kar Han Tan)

we follow with a formal analysis of this intuition by evaluating the conditioning of the discrete forward model (Eq. 4). We also evaluate the contrast of generated imagery and analyze extensions of lateral and axial viewing ranges for an observer.

**Intuition** Figure 4 (a) shows an example of a prefiltered light field with  $3 \times 3$  views for a sample scene. In this example, the different views contain overlapping parts of the target image (yellow box), allowing for increased degrees of freedom for aberration compensation. Precisely these degrees of freedom are what makes the problem of correcting visual aberrations well-posed. The 4D prefiltering does not act on a 2D image, as is the case for conventional displays, but lifts the problem into a higher-dimensional space in which it becomes invertible. Although the prefiltered light field (Fig. 4, a) appears to contain amplified high frequencies in each view of the

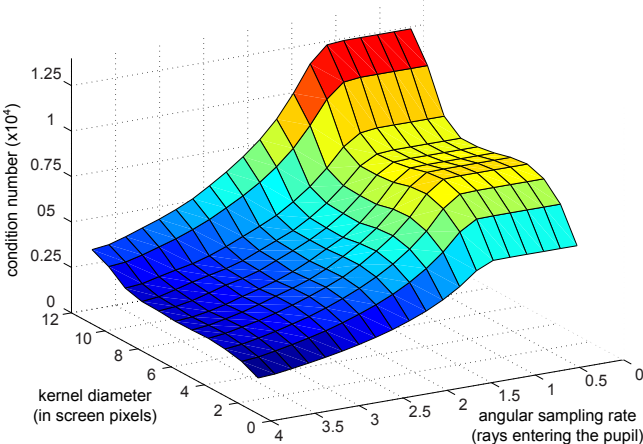


**Figure 5:** Conditioning analysis. The light field projection matrix corresponding to a defocused eye is ill-conditioned. With more angular resolution available in the emitted light field, more degrees of freedom are added to the system, resulting in lower condition numbers (lower is better). The condition number of the projection matrix is plotted for a varying defocus distance (kernel size) and angular resolution (number of light field views). We observe that even as few as 1.5 angular light field samples entering the pupil of an observer decrease the condition number.

light field, the prefilter actually acts on all four dimensions simultaneously. When optically projected onto the retina of an observer, all light field views are averaged, resulting in a perceived image that has significantly improved sharpness (c) as compared to an image observed on a conventional 2D display (b).

We illustrate this principle using an intuitive 2D light field in Figures 4 (d-g). The device emits a light field with three (d,e) and five (f,g) views, respectively. Individual views are shown in different colors. These are sheared in display space (d,f), because the eye is not actually focused on the display due to the constrained accommodation range of the observer. The finite pupil size of the eye limits the light field entering the eye, as illustrated by the semi-transparent white regions. Whereas we show the light fields in both display coordinates (d,f) and eye (e,g) coordinates, the latter is more intuitive for understanding when vision correction is possible. For locations on the retina that receive contributions from multiple different views of the light field (indicated by yellow boxes in e,g), the inverse problem is well-posed. Regions on the retina that only receive contributions from a single light field view, however, are optically equivalent to the conventional 2D display case, which is ill-posed for vision correction.

**Conditioning Analysis** To formally verify the discussed intuition, we analyze the condition number of the light field projection matrix  $\mathbf{P}$  (see Eqs. 4, 5). Figure 5 shows the matrix conditioning for varying amounts of defocus and angular light field resolution (lower condition number is better). Increasing the angular resolution of the light field passing through the observer’s pupil significantly decreases the condition number of the projection matrix for all amounts of defocus. This results in an interesting observation: *increasing the amount of defocus increases the condition number but increasing the angular sampling rate does the opposite*. Note that the amount of defocus is quantified by the size of a blur kernel on the screen (see Fig. 5).

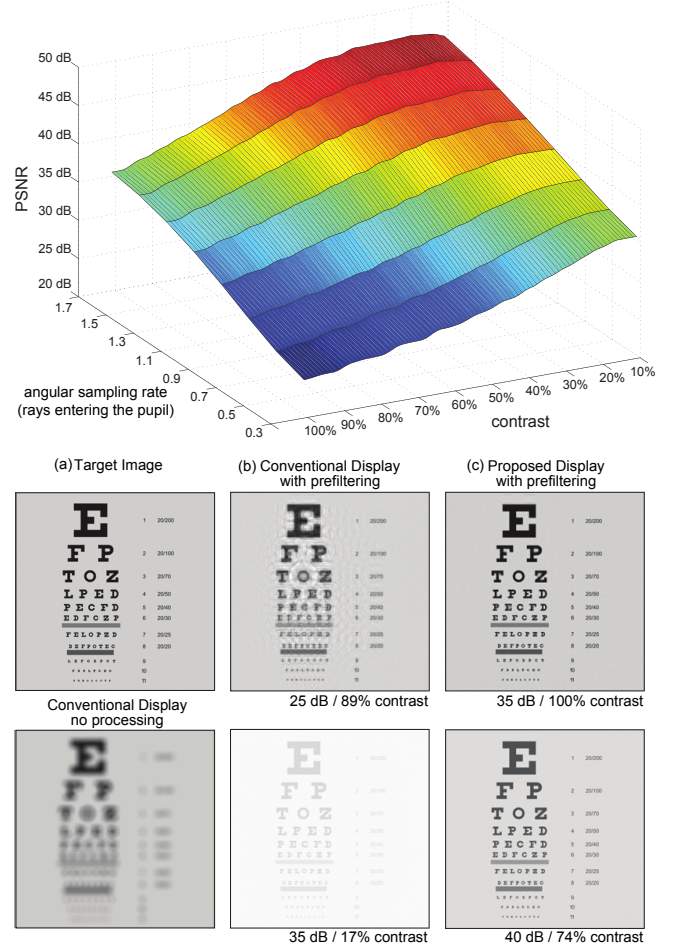


**Figure 6:** Tradeoff between angular light field resolution and image contrast. Top: we reconstruct a test image with different combinations of angular resolution and image contrast and plot the achieved PSNR. Bottom: using prefiltering with a conventional 2D display (b), we obtain either a low-quality but high-contrast image or a high-quality but low-contrast image. For a light field display with 1.5 or more prefiltered views entering the pupil (c), a similar trend is observed but overall reconstruction quality is significantly increased. (Snellen chart courtesy of Wikipedia user Jeff Dahl)

The condition number drops significantly after it passes the 1.3 mark, where the angular sampling enables more than one light field view to enter the pupil. This effectively allows for angular light field variation to be exploited in the prefiltering. As more than two light field views pass through the pupil, the condition number keeps decreasing but at a much slower rate. With an extreme around 7 to 9 views, the system becomes the setup of Pamplona et al.: each ray hits exactly one retinal pixel, but the spatial-angular trade-off reduces the image resolution. Our light field prefiltering method is located in between these two extremes of choosing either high resolution or high contrast, but never both simultaneously. Usually, less than two views are required to maintain a sufficiently low condition number. The experiments in Figure 5 are computed with a viewing distance of 350mm, a pupil diameter of 6mm, and a pixel pitch of 45 $\mu\text{m}$ . The angular sampling rate refers to the number of light field views entering the pupil.

**Image Contrast Optimization** At the defocus level shown in Figure 6 (a, bottom), naively applying the nonnegative constraint

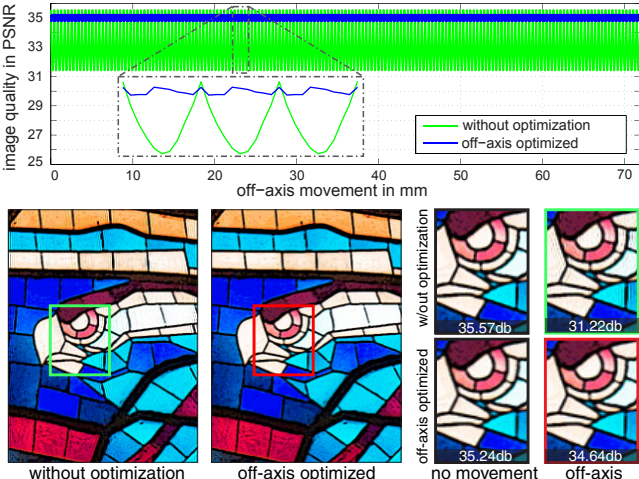


**Figure 7:** Compensating for a range of lateral viewpoints. Aberration-free image display is possible when the relative position of the eye with respect to the display is known. The green plot evaluates image degradation for viewpoints that deviate laterally from the sweetspot. Only slight ringing is visible and, due to periodic viewing zones of the employed parallax barrier display, image quality varies in a periodic manner (top, zoom-in). We can account for a range of perspectives in the compensation, ensuring high image quality for a wider viewing range (blue plot). The columns on the bottom right show on-axis and off-axis views with and without accounting for a range of lateral viewpoints in the optimization. (Source image courtesy of Wikipedia user Lexaxis7)

in Equation 5 results in additional artifacts as shown in (b, top). Alternatively, we can shift and scale the target image before solving the system, effectively scaling the target image into the range space of the projection matrix. Although this is a user-defined process, observed image quality can be enhanced. In particular, Equation 5 can be modified as

$$\begin{aligned} \text{minimize}_{\{l_i^d\}} \quad & \|(\mathbf{i} + b)/(1 + b) - \mathbf{P}\mathbf{l}^d\|_2 \\ \text{subject to} \quad & 0 \leq l_i^d \leq 1, \quad \text{for } i = 1 \dots N \end{aligned} \quad (11)$$

where  $b$  is a user specified bias term that reduces the image contrast to  $1/(b+1)$ .

We plot achieved image quality measured in PSNR for all contrast levels at various angular sampling rates in Figure 6 (top). With a conventional display, prefiltering results in ringing artifacts (b) because the inverse problem is ill-conditioned. Artificially reducing the image contrast mitigates the artifacts but makes the text illegible (b, bottom). A light field display makes the inverse problem well-posed, allowing for high quality prefiltering (c). The pixel pitch of the experiment shown in Figure 6 is 96 $\mu\text{m}$ ; other parameters are the same as in Figure 5. Please note that the contrast bias term  $b$  may require manual tuning for each experiment.

**Extending Lateral and Axial Viewing Range** We envision most future display systems that incorporate vision-correcting technologies to use eye tracking. In such devices, the projection matrix (see Eq. 4) is dynamically updated for the perspective of the observer. For applications in emerging near-eye displays [Lanman and Luebke 2013], on the other hand, the proposed technology would not require eye-tracking because the relative position between eye and display is fixed. Within the context of this paper, we assume that eye tracking is either available or the relative position between display and eye is fixed.

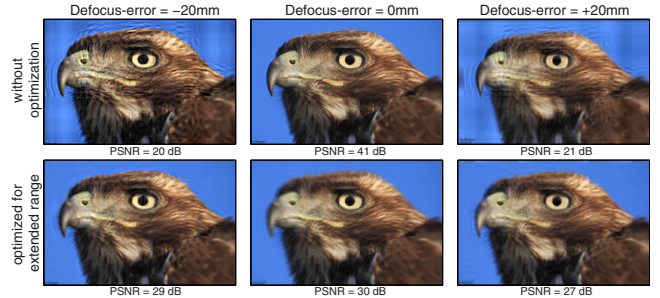


**Figure 8:** Accounting for a range of viewing distances. Top row: when considering a fixed viewing distance, defocus errors are compensated at that exact distance (top center) but image quality degrades when the observer moves forward or back (top left and right). The proposed method can account for a range of viewing distances (bottom row), which slightly degrades quality at the sweetspot but significantly improves all other distances. (Source image courtesy of Kar Han Tan)

Nevertheless, we evaluate image degradation for viewpoints that are at a lateral distance from the target viewpoint in Figure 7. Such shifts could be caused by imprecise tracking or quickly moving observers. We observe slight image degradation in the form of ringing. However, even the degraded image quality is above 30 dB in this experiment and varies in a periodic manner (Fig. 7, top: zoom-in). This effect can be explained by the periodic viewing zones that are created by the employed parallax barrier display; a similar effect would occur for lenslet-based light field displays. We can account for a range of lateral viewpoints by changing the matrix in Equation 11 to  $\mathbf{P} = [\mathbf{P}_{\mathbf{T}_1} \dots \mathbf{P}_{\mathbf{T}_M}]^T$ , where each  $\mathbf{P}_{\mathbf{T}_i}$  is the projection matrix of one of  $M$  perspectives. Although this approach slightly degrades image quality for the central sweetspot, a high image quality (approx. 35 dB) is achieved for a much wider range of viewpoints. The lateral range tested in Figure 7 is large enough to demonstrate successful aberration-correction for binocular vision, assuming that the inter-ocular distance is approx. 65 mm. Please also refer to additional experiments in the supplemental video.

We also show results for a viewer moving along the optical axis in Figure 8. Just like for lateral motion, we can account for variable distances by stacking multiple light field projection matrices into Equation 11 with incremental defocus distances. The resulting equation system becomes over-constrained, so the solution attempts to satisfy all viewing distances equally well. This results in slight image degradations for the sweetspot, but significantly improves image quality for all other viewing distances.

## 5 Implementation and Results

The proposed aberration-correcting display can be implemented using most light field display technologies. For the purpose of this paper, we demonstrate the feasibility of our techniques with a parallax barrier display [Ives 1903], because the required hardware is readily available and inexpensive. Please note that the proposed displays are not limited to this particular architecture, although the image formation (Eq. 4) has to be adjusted for any particular setup.

**Hardware** The prototype is shown in Figure 9. A pinhole-based parallax barrier mask is printed with 5080 DPI on a transparency with a Heidelberg Herkules imagesetter ([www.pageworks.com](http://www.pageworks.com)). To optimize light throughput and avoid diffraction, the pinholes have a size of 75 microns each and are spaced 390 microns apart. This mask is mounted at an offset of 5.4 mm in front of a conventional

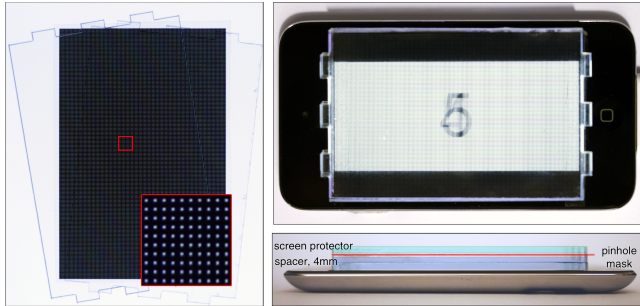


**Figure 9:** Prototype display. We construct an aberration-correcting display using parallax barriers. The barrier mask contains a pinhole array (left) that is mounted at a slight offset in front of an Apple iPod touch 4 screen (lower right). The display emits a light field with a high-enough angular resolution so that at least two views enter the pupil of a human observer. This effect is illustrated on the top right: multiple Arabic numerals are emitted in different viewing directions; the finite pupil size then creates an average of multiple different views on the retina (here simulated with a camera).

2D screen using a clear acrylic spacer. The screen is an Apple iPod touch 4th generation display with a pixel pitch of 78 microns (326 PPI) and a total resolution of  $960 \times 640$  pixels.

The dimensions of our prototype allow 1.66 light field views to enter a human pupil with a diameter of 6 mm at a distance of 25 cm. Higher-resolution panels are commercially available and would directly improve spatial and angular resolution and also facilitate larger viewing distances.

**Software** The light field prefiltering algorithm is implemented in Matlab on a PC with a 2.7GHz 2-core CPU and 8GB of RAM. The projection matrix is precomputed in about 3 minutes with radians sampling the pupil at 20 rays/mm, resulting in approx. 11,300 effective rays per retinal pixel. We use the non-negative least squares solver package *LBFGB* [Byrd et al. 1995] to solve Equation 11 in about 20 seconds for each image shown on the prototype. The projection matrix only needs to be computed once for each viewing distance and we believe that an optimized GPU implementation of the solver could achieve real-time framerates.

**Photographs of Prototype** We show a variety of results captured from our prototype display in Figure 10 (center right column). These photographs are captured with a Canon T3i DSLR camera equipped with a 50 mm lens at f/8. The display is placed at a distance of 25 cm to the camera. The camera is focused at 38 cm, placing the screen 13 cm away from the focal plane. This camera closely resembles a -6D hyperopic human eye.

Figure 10 (right column) shows the simulated results corrected with our techniques. The results captured from the prototype (Fig. 10, third column) closely resemble these simulations but contain minor artifacts that are due to moiré between the barrier mask and the display pixels. Compared to conventional 2D images shown on the screen (Fig. 10, first column), image sharpness is significantly improved without requiring the observer to wear glasses. We also compare our approach to the method proposed by Pamplona et al. [2012] for the same display resolution and spatio-angular tradeoff (Fig. 10, second column). Basically, their approach uses the same display setup as ours but a direct solution rather than the proposed prefilter. Our approach outperforms their method and allows for significantly increased resolution.

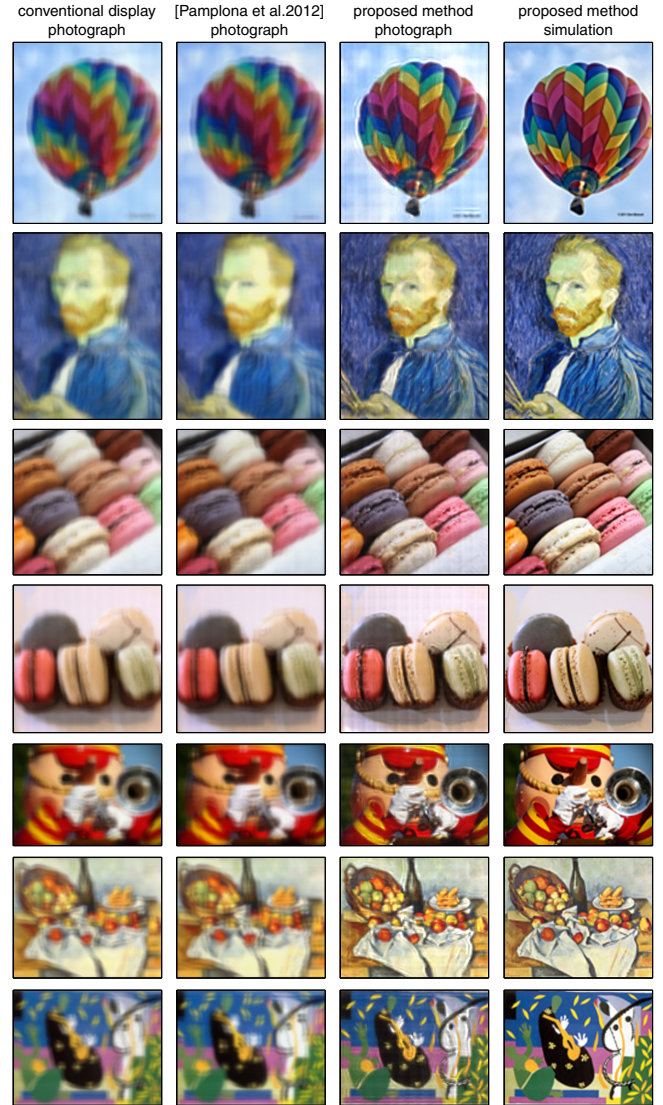


**Figure 10:** Photographs of prototype display. The hyperopic camera simulates a human pupil with a diameter of 6 mm at a distance of 25 cm to the screen. Focused at 38 cm, images shown on a conventional screen are blurred (first column). While previous methods theoretically facilitate increased image sharpness (second column), achievable resolution is fundamentally limited by the spatio-angular resolution tradeoff of the required light field display. Light field prefiltering, as proposed in this paper, allows for significantly increased resolutions (third column). The prototype closely resembles simulations (right column). (From top, source images courtesy of *dfbphotos* (flickr), *Vincent van Gogh*, *Houang Stephane* (flickr), *JFXie* (flickr), *Jameziecakes* (flickr), *Paul Cezanne*, *Henri Matisse*)

## 6 Evaluation

### 6.1 Visual Performance

We evaluate achieved quality in Figure 11. For this experiment, we simulate a 10 inch tablet with a 300 PPI panel and the pinhole parallax barrier with 6.5 mm offset. The tablet is held at a distance of 30 cm and viewed with a -6.75D hyperopic eye; images are shown on the center of the display in a  $10.8 \text{ cm} \times 10.8 \text{ cm}$  area. For each example, we compare our approach with the direct light

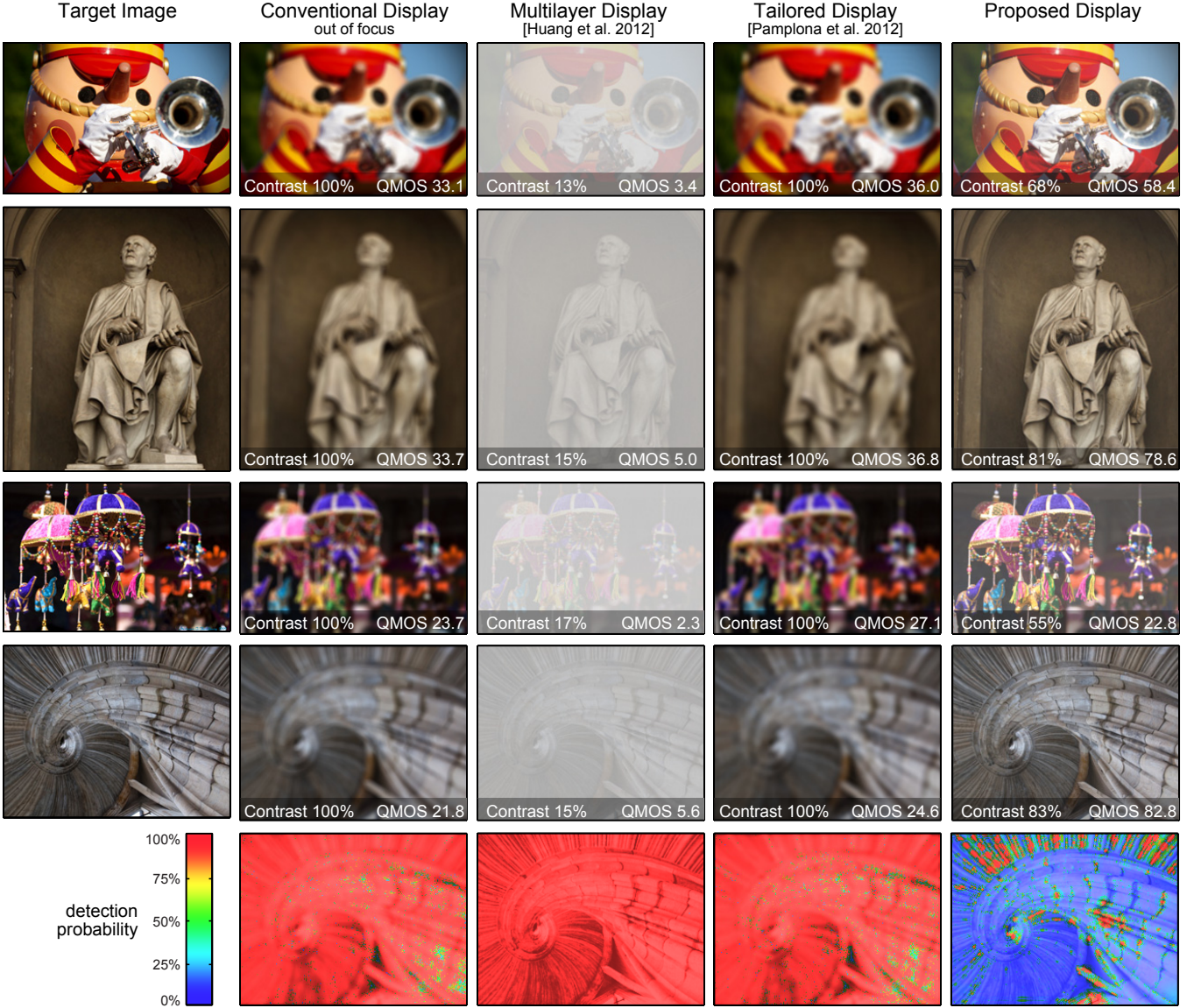


**Figure 11:** Evaluation and comparison to previous work. We compare simulations of conventional and vision-correcting image display qualitatively and quantitatively using contrast and quality-mean-opinion-square (QMOS) error metrics. A conventional out-of-focus display always appears blurred (second column). Multilayer displays with prefiltering improve image sharpness but at a much lower contrast (third column). Light field displays without prefiltering require high angular resolutions, hence provide a low spatial resolution (fourth column). The proposed method combines prefiltering and light field display to optimize image contrast and sharpness (right column). The QMOS error metric is a perceptually linear metric, predicting perceived quality for a human observer. We also plot maps that illustrate the probability of an observer detecting the difference of a displayed image to the target image (bottom row). Our method performs best in most cases. (Source images courtesy of Jameziecakes (flickr), Kar Han Tan, Mostaque Chowdhury (flickr), and Thomas Quine (flickr))

field approach and multilayer prefiltering. The target contrast for prefiltering methods is manually adjusted to achieve the best PSNR for each example.

**Contrast Metric** Prefiltering involves modulating the image content by enhancing weaker frequencies. Without utilizing the full degrees of freedom in the light field sense, the results obtained using multilayer prefiltering suffer from extreme contrast loss, here measured in Michelson contrast. This is defined as  $(I_{max} - I_{min})/(I_{max} + I_{min})$ , where  $I_{max,min}$  are the maximum and minimum intensity in the image, respectively. Light field predistortion does not depend on content modifications but on resampling of the light field, so the contrast is not sacrificed. By efficiently using all

views, the proposed light field prefiltering approach restores contrast by a factor of 3 to 5× higher than that of the multilayer prefiltering. We note that the contrast achieved with light field prefiltering is not quite as good as the raytracing algorithm, which always gives full contrast. However, when closely inspecting the image content, the raytracing solution always results in blurred images, which is due to insufficient spatial resolution.

**Perceptual Metric** To assess both contrast and sharpness, we resort to HDR-VDP2 [Mantiuk et al. 2011], a perceptually-based image metric. The quality mean opinion score (QMOS) gives an evaluation of overall perceived image quality, and in most examples we score 2 to 3 times higher than other approaches. The images

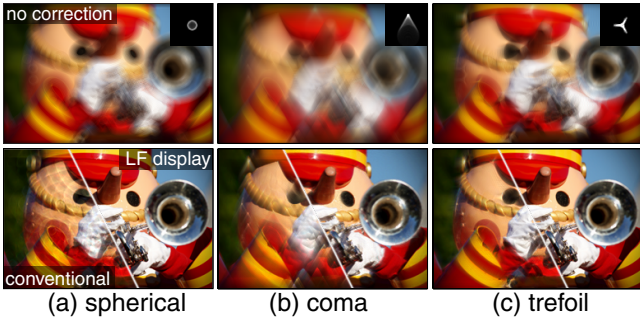


**Figure 12:** Correcting for higher-order aberrations. We simulate images observers with different types of higher-order aberrations perceive (top row) and show corresponding point spread functions (top row, insets), which exhibit a range of different shapes. Most of them are difficult to compensate with a conventional 2D display (bottom row, lower left parts), although the blur kernel associated with trefoil (lower right) is frequency preserving and therefore invertible. The proposed aberration-correcting display is successful in compensating all of these aberrations (bottom row, upper right parts). (Source image courtesy of flickr user Jameziecakes)

in the third row are a particularly difficult example for prefiltering-based algorithms, because performance depends on the frequency content of the image which, in this case, does not allow prefiltering to achieve a higher quality. Lots of high frequencies in the example tend to reduce image contrast so that even our light field prefiltering scores slightly lower. Visually, our result still looks sharp. In the last row of Figure 11, we show a probabilistic map on whether a human can detect per pixel differences for the fourth example. Clearly, our result has a much lower detection rate.

Note that the reduced image sharpness of conventional displays (Fig. 11, column 2) is due to defocus blur in the eye, whereas that of Tailored Displays (Fig. 11, column 4) is due to the low spatial resolution of the light field display. All displays in this simulation have the same pixel count, but the microlens array used in Tailored Displays trades spatial display resolution for angular resolution. Our solution also has to trade some spatial resolution, but due to the prefiltering method we basically optimize this tradeoff.

## 6.2 Correcting Higher-Order Aberrations

Although aberrations of human eyes are usually dominated by myopia and hyperopia, astigmatism and higher-order aberrations may also degrade observed image quality. Visual distortions of a perceived wavefront are usually described by a series of basis functions known as Zernike polynomials. These are closely related to spherical harmonics, which are commonly used in computer graphics applications. Lower-order Zernike polynomials include defocus and astigmatism whereas higher-order terms include coma, trefoil, spherical aberrations, and many others. The effects of any such terms can easily be incorporated into the image inversion described in Section 3 by modifying the projection matrix  $\mathbf{P}$ .

Figure 12 evaluates compensation of higher-order aberrations with the proposed approach. The top row shows the images an observer with these aberrations perceives without correction. Just as in the case of defocus, prefiltering for a conventional display usually fails to achieve high image quality (bottom row, lower left image parts). We observe ringing artifacts that are typical for solving ill-posed deconvolution problems. The proposed aberration-correcting display, on the other hand, successfully compensates for all types of aberrations (bottom row, upper right parts). What is particularly interest-

ing to observe in this experiment is that some types of higher-order aberration can be reasonably well compensated with a conventional display. As seen in the right column of Figure 12 (bottom row, lower left part), the point spread function of trefoil, for example, is frequency preserving and therefore easy to invert. For most other types of aberrations, however, this is not the case. Extended experiments including astigmatism and additional higher-order aberrations can be found in the supplemental document.

## 7 Discussion

In summary, we present a computational display approach to correcting low and high order visual aberrations of a human observer. Instead of wearing vision-correcting glasses, the display itself pre-distorts the presented imagery so that it appears as a desired target image on the retina of the observer. Our display architecture employs off-the-shelf hardware components, such as printed masks or lenslet arrays, combined with computational light field prefiltering techniques.

We envision a wide range of possible implementations on devices such as phones, tablets, televisions, and head-worn displays. In this paper, we demonstrate one particular implementation using a low-cost hardware add-on to a conventional phone. In a commercial setting, this could be implemented using switchable liquid crystal barriers, similar to those used by Nintendo 3DS, which would allow the display to dynamically adapt to different viewers or viewing conditions.

The proposed techniques assume that the precise location of the observer’s eye w.r.t. the screen is either fixed or tracked. Robust solutions to eye tracking, however, are not a contribution of this paper. Each of the envisioned display types provides different challenges for tracking pupils. For generality, we focus discussions on the challenges of correcting vision. Inexpensive eye trackers are commercially available today (e.g., <http://theeyetribe.com>) and could be useful for larger-scale vision-correcting displays; hand-held devices could use integrated cameras. Nevertheless, we evaluate strategies to account for a range of viewer motion, which could not only help decrease jittering of existing trackers but also remove the need for tracking in some applications.

**Benefits and Limitations** The proposed techniques offer significantly increased resolution and contrast compared to previously-proposed vision-correcting displays. Intuitively, light field prefiltering minimizes demands on angular light field resolution, which directly results in higher spatial resolution. For device implementations with lenslet arrays, the reduced angular resolution, compared to Pamplona et al. [2012], allows for shorter focal lengths of the employed lenslets resulting in thinner form factors and easier fabrication. For implementations with parallax barriers, pinhole spacings are reduced allowing for increased image brightness.

We treat lenslet arrays and parallax barriers as very similar optical elements throughout the manuscript. In practice, the image formation is slightly different and the implementation of Equation 4 is adjusted for each case. As outlined in Section 1, the proposed system requires increased computational resources and modifications to conventional display hardware. Nevertheless, we demonstrate that an inexpensive hardware attachment for existing phones is sufficient to build the required device. Whereas the parallax barriers in our prototype are relatively light inefficient, lenslet arrays could overcome this limitation. Our current Matlab implementation does not support interactive frame rates. Real-time GPU implementations of similar problems [Wetzstein et al. 2012], however, are a strong indicator that interactive framerates could also be achieved for the proposed methods.

While the proposed approach provides increased resolution and contrast as compared to previous approaches, achieving the full target image resolution and contrast is not currently possible. We evaluate all system parameters and demonstrate prototype results under conditions that realistically simulate a human pupil; however, we do not perform a user study. Slight artifacts are visible on the prototype, these are mainly due to limitations in how precisely we can calibrate the distance between the pinhole mask and screen pixels, which are covered by protective glass with an unknown thickness. As artifact-free light field displays resembling the prototype setup are widely available commercially, we believe that the observed artifacts could be removed with more engineering efforts. The parameter  $b$  in Section 4 is manually chosen, but could be incorporated into the optimization, making the problem more complex. We leave this formulation for future research.

**Future Work** We show successful vision-correction for a variety of static images and precomputed animations. In the future, we would like to explore real-time implementations of the proposed techniques that support interactive content. Emerging compressive light field displays (e.g., [Wetzstein et al. 2012; Maimone et al. 2013]) are promising architectures for high-resolution display—vision-correcting devices could directly benefit from advances in that field. In the long run, we believe that flexible display architectures will allow for multiple different modes, such as glasses-free 3D image display, vision-corrected 2D image display, and combinations of vision-corrected and 3D image display. We would like to explore such techniques.

## 8 Conclusion

Correcting for visual aberrations is critical for millions of people. Today, most of us spend a significant amount of time looking at computer screens on a daily basis. The computational display designs proposed in this paper could become a transformative technology that has a profound impact on how we interact with digital devices. Suitable for integration in mobile devices, computer monitors, and televisions, our vision-correcting displays could become an integral part of a diverse range of devices. Tailoring visual content to a particular observer may very well turn out to be the most widely used application of light field displays. Combined with glasses-free 3D display modes, the proposed techniques facilitate a variety of novel applications and user interfaces that may revolutionize user experiences.

## Acknowledgements

This research was supported in part by the National Science Foundation at the University of California, Berkeley under grant number IIS-1219241, “Individualized Inverse-Blurring and Aberration Compensated Displays for Personalized Vision Correction with Applications for Mobile Devices”, and at MIT under grant number IIS-1116718, “AdaCID: Adaptive Coded Imaging and Displays”. Gordon Wetzstein was supported by an NSERC Postdoctoral Fellowship. The authors wish to thank Dr. Douglas Lanman and Prof. Austin Roorda for early feedback and discussions.

## References

- AKELEY, K., WATT, S. J., GIRSHICK, A. R., AND BANKS, M. S. 2004. A stereo display prototype with multiple focal distances. *ACM Trans. Graph. (SIGGRAPH) 23*, 3, 804–813.
- ALONSO JR., M., AND BARRETO, A. B. 2003. Pre-compensation for high-order aberrations of the human eye using on-screen im-
- age deconvolution. In *IEEE Engineering in Medicine and Biology Society*, vol. 1, 556–559.
- ARCHAND, P., PITE, E., GUILLEMET, H., AND TROCME, L., 2011. Systems and methods for rendering a display to compensate for a viewer’s visual impairment. International Patent Application PCT/US2011/039993.
- BYRD, R. H., LU, P., NOCEDAL, J., AND ZHU, C. 1995. A limited memory algorithm for bound constrained optimization. *SIAM J. Sci. Comput. 16*, 5 (Sept.), 1190–1208.
- CHAI, J.-X., TONG, X., CHAN, S.-C., AND SHUM, H.-Y. 2000. Plenoptic sampling. In *ACM SIGGRAPH*, 307–318.
- COSSAIRT, O. S., NAPOLI, J., HILL, S. L., DORVAL, R. K., AND FAVALORA, G. E. 2007. Occlusion-capable multiview volumetric three-dimensional display. *Applied Optics 46*, 8, 1244–1250.
- DURAND, F., HOLZSCHUCH, N., SOLER, C., CHAN, E., AND SILLION, F. X. 2005. A frequency analysis of light transport. In *Proc. SIGGRAPH*, 1115–1126.
- GORTLER, S. J., GRZESZCZUK, R., SZELISKI, R., AND COHEN, M. F. 1996. The lumigraph. In *Proc. SIGGRAPH, SIGGRAPH ’96*, 43–54.
- HECHT, E. 2001. *Optics (Fourth Edition)*. Addison-Wesley.
- HIRSCH, M., WETZSTEIN, G., AND RASKAR, R. 2014. A compressive light field projection system. *ACM Trans. Graph. (SIGGRAPH) 33*.
- HUANG, F.-C., AND BARSKY, B. 2011. A framework for aberration compensated displays. *Tech. Rep. UCB/EECS-2011-162, University of California, Berkeley, December*.
- HUANG, F.-C., LANMAN, D., BARSKY, B. A., AND RASKAR, R. 2012. Correcting for optical aberrations using multilayer displays. *ACM Trans. Graph. (SIGGRAPH Asia) 31*, 6, 185:1–185:12.
- IVES, F. E., 1903. Parallax stereogram and process of making same. U.S. Patent 725,567.
- JONES, A., McDOWALL, I., YAMADA, H., BOLAS, M., AND DEBEVEC, P. 2007. Rendering for an interactive 360° light field display. *ACM Trans. Graph. (SIGGRAPH) 26*, 40:1–40:10.
- LANMAN, D., AND LUEBKE, D. 2013. Near-eye light field displays. *ACM Trans. Graph. (SIGGRAPH Asia) 32*, 6, 220:1–220:10.
- LANMAN, D., HIRSCH, M., KIM, Y., AND RASKAR, R. 2010. Content-adaptive parallax barriers: optimizing dual-layer 3D displays using low-rank light field factorization. *ACM Trans. Graph. 29*, 163:1–163:10.
- LEVIN, A., HASINOFF, S. W., GREEN, P., DURAND, F., AND FREEMAN, W. T. 2009. 4D frequency analysis of computational cameras for depth of field extension. *ACM Trans. Graph. (SIGGRAPH) 28*, 3.
- LEVOY, M., AND HANRAHAN, P. 1996. Light field rendering. In *Proc. SIGGRAPH*, 31–42.
- LIPPMANN, G. 1908. Épreuves réversibles donnant la sensation du relief. *Journal of Physics 7*, 4, 821–825.
- LOVE, G., HOFFMAN, D., HANDS, P., GAO, J., KIRBY, A., AND BANKS, M. 2009. High-speed switchable lens enables the development of a volumetric stereoscopic display. *Optics Express 17*, 15716–15725.

MAIMONE, A., WETZSTEIN, G., HIRSCH, M., LANMAN, D., RASKAR, R., AND FUCHS, H. 2013. Focus 3d: Compressive accommodation display. *ACM Trans. Graph.* 32, 5, 153:1–153:13.

MANTIUK, R., KIM, K. J., REMPEL, A. G., AND HEIDRICH, W. 2011. Hdr-vdp-2: a calibrated visual metric for visibility and quality predictions in all luminance conditions. In *Proc. ACM SIGGRAPH*, 40:1–40:14.

MASIA, B., WETZSTEIN, G., DIDYK, P., AND GUTIERREZ, D. 2013. A survey on computational displays: Pushing the boundaries of optics, computation, and perception. *Computers & Graphics* 37, 8, 1012–1038.

NG, R., AND HANRAHAN, P. 2006. Digital correction of lens aberrations in light field photography. In *Proc. SPIE International Optical Design*.

NG, R. 2005. Fourier slice photography. In *ACM SIGGRAPH 2005 Papers*, ACM, New York, NY, USA, SIGGRAPH '05, 735–744.

PAMPLONA, V. F., MOHAN, A., OLIVEIRA, M. M., AND RASKAR, R. 2010. Netra: interactive display for estimating refractive errors and focal range. *ACM Trans. Graph. (SIGGRAPH)* 29, 77:1–77:8.

PAMPLONA, V. F., PASSOS, E. B., ZIZKA, J., OLIVEIRA, M. M., LAWSON, E., CLUA, E., AND RASKAR, R. 2011. Catra: interactive measuring and modeling of cataracts. *ACM Trans. Graph. (SIGGRAPH)* 30, 4, 47:1–47:8.

PAMPLONA, V., OLIVEIRA, M., ALIAGA, D., AND RASKAR, R. 2012. Tailored displays to compensate for visual aberrations. *ACM Trans. Graph. (SIGGRAPH)* 31.

RAMAMOORTHI, R., MAHAJAN, D., AND BELHUMEUR, P. 2007. A first-order analysis of lighting, shading, and shadows. *ACM Trans. Graph.* 26, 1.

TAKAKI, Y. 2006. High-Density Directional Display for Generating Natural Three-Dimensional Images. *Proc. IEEE* 94, 3.

VITALE, S., SPERDUTO, R. D., AND FERRIS, III, F. L. 2009. Increased prevalence of myopia in the United States between 1971–1972 and 1999–2004. *Arch. Ophthalmology* 127, 12, 1632–1639.

WETZSTEIN, G., LANMAN, D., HEIDRICH, W., AND RASKAR, R. 2011. Layered 3D: tomographic image synthesis for attenuation-based light field and high dynamic range displays. *ACM Trans. Graph. (SIGGRAPH)* 30, 4.

WETZSTEIN, G., LANMAN, D., HIRSCH, M., AND RASKAR, R. 2012. Tensor displays: Compressive light field synthesis using multilayer displays with directional backlighting. *ACM Trans. Graph. (SIGGRAPH)* 31.

WONG, T. Y., FOSTER, P. J., HEE, J., NG, T. P., TIELSCH, J. M., CHEW, S. J., JOHNSON, G. J., AND SEAH, S. K. 2000. Prevalence and risk factors for refractive errors in adult chinese in singapore. *Invest Ophthalmol Vis Sci* 41, 9, 2486–94.

YELLOTT, J. I., AND YELLOTT, J. W. 2007. Correcting spurious resolution in defocused images. *Proc. SPIE* 6492.